Defence Science Journal, Vol. 71, No. 2, March 2021, pp. 185-191, DOI : 10.14429/dsj.71.15965

Hematite Suspension based Absorbent Pad Inclined Slider Influenced by Slip and Squeeze Velocity with Altering Film Ratio

Paras Ram and Anil Kumar*

Department of Mathematics, National Institute of Technology, Kurukshetra - 136 119, India
**E-mail: anilkumar6150013@gmail.com*

ABSTRACT

The effects of various entities like slip and squeeze velocities, inlet-outlet film ratio, and the material parameter have been fairly explored in a hematite suspension based absorbent (porous) pad inclined slider. Mathematical expressions for pressure, load capacity (lifting force), friction, friction coefficient, and position of centre of pressure (COP) in terms of the above physical parameters have been acquired. Jenkins model has been employed as a mathematical set of governing equations. It has been found that an increase in the squeeze velocity has enhanced the load capacity and diminished the friction coefficient whereas the escalating values of slip velocity and material properties have reversed the trends. Besides, the optimum value of the inlet-outlet film ratio for maximum load capacity has reduced with a rise in the squeeze velocity. Improvement in material parameters shifted the position of COP slightly towards the inlet while an enhancement in the squeeze velocity and film ratio shifted the same slightly towards the outlet. The results acquired in the present paper will be helpful in designing and modifying the various types of fluid dynamic slider bearings.

Keywords: Slip velocity; Squeeze velocity; Inlet-outlet ratio or Film ratio; Load capacity or lifting force; Friction; Centre of pressure

NOMENCLATURE

λ^2	Material parameter
$\overline{\lambda}^2$	Dimensionless material parameter
ε	Permeability parameter
$\overline{\varepsilon}$	Dimensionless permeability parameter
β	Material constant
ρ	Fluid density
μ_v	Coefficient of viscosity
μ_o	Permeability of Free space
$\overline{\mu}_m$	Dimensionless magnetic parameter
μ_s	Magnetic susceptibility
χ_0	Initial susceptibility of fluid
$\tilde{M}$	Magnetisation vector
M	Magnitude of magnetisation vector
M_s	Saturation magnetisation
M^*	Co-rotational derivative of magnetisation
$1/\overline{\tau}$	Dimensionless slip parameter
τ	Slip parameter
$r_{i/o}$	Inlet-outlet film ratio
F	External mag. field strength
$\hbar$	Film's height
$\hbar_0$	Min. film's thickness
$\hbar_1$	Max. film's thickness
$\overline{\hbar}$	Dimensionless film's height
κ	Porous matrix's porosity
l	Bearing's wall thickness
L	Bearing's width
P_r	Fluid's pressure
p_r	Porous region's pressure
$\overline{P}_r$	Dimensionless fluid pressure
(x, y)	Cartesian's coordinates
$\overline{x}$	Dimensionless x-coordinate
V_x	Velocity component/factor along x-axis
v_x	Velocity factor along x-axis in the porous region
V_y	Velocity factor along y-axis
v_y	Velocity factor along y-axis in the porous region
U_x	Uniform or regular sliding velocity factor with x-axis
$\vec{V}$	Fluid's velocity
V_{sq}	Squeeze velocity
$\overline{V}_{sq}$	Dimensionless squeeze velocity
$\overline{A}$	Defined as in Eqn (27)
$\overline{B}$	Defined as in Eqn (28)
$\overline{C}$	Defined as in Eqn (31)
$\overline{W}$	Dimensionless load capacity
$\overline{F}_r$	Dimensionless friction
$\overline{f}_r$	Dimensionless friction coefficient
$\overline{C}_p$	Dimensionless position of centre of pressure (COP)

Received : 27 May 2020, Revised : 30 October 2020
Accepted : 04 February 2021, Online published : 10 March 2021

1. INTRODUCTION

Ferrofluids (FFs) more commonly known as magnetic fluids are a special class of synthesised fluids, which shows noteworthy variations in its flow behaviour under the effect of an externally applied oblique magnetic field. It contains fine ferro-magnetic particles such as Fe_2O_3 (Hematite), Fe_3O_4

(Magnetite), $Ni-Fe$, Co etc. dispersed in a base fluid called carrier liquid. These particles are coated with a surfactant to prevent clumping. Each tiny particle of hematite/magnetite can be treated as a permanent magnet with a high magnetic moment. Initially iron content in magnetite is more as compared to hematite. However, during machine operation where temperature rises due to friction (between pads of the slider bearing), there is a quite gain in the magnetisation of hematite particles. Also, hematite is more abundant in nature than magnetite so is economical.

Due to an external oblique magnetic field, FFs experience magnetic body forces. The magnitude of such forces depends upon the magnetisation of ferro particles. Long term stability and faster rate of heat transfer[1,2] of FFs have fascinated the researchers dealing with the problems of various geometries like slider planer motion[3] table, rotating disk[4–6], circular disks[7,8] helical pipes[9], etc. Ferro fluid lubrication[10] plays an imperative role to enhance the heat transfer rate and the lifting force in thrust bearings[11–13], journal bearings[14–17], conical bearings[18], inclined slider bearings[19,20], exponential slider bearings[21], ball bearings[22] and textured rolling bearing[23].

Shah & Bhatt[24] found that the Jenkins model is more realistic since it deals with the material used in the bearing design. Agrawal[25] investigated that the magnetic factor improved the bearing's load capacity without affecting the friction. Ram &Verma[26] extended Agarwal's work and concluded that load capacity further enhances with the escalating values of magnetic factor and the material parameter. Ram[27], *et al*. studied that the film ratio plays a vital role to affect the lifting force and found its optimum value for which the lifting force was maximum.

The present paper is an extension of the work done by Shah & Bhatt[24], Ram &Verma[26] and Ram[27], *et al.*. These researchers analysed the load capacity of the slider bearing for zero squeeze velocity. Shah & Bhatt[24] and Ram &Verma[26] considered a particular value of the film ratio and hence did not studied the effects of altering film ratio on bearing performance. Ram[27], *et al.* considered this gap but they did not give stress on the factors affecting the optimum value of the film ratio for maximum load capacity. Therefore, these gaps together with the squeeze velocity have been considered in the present paper, and the combined effects of all the above-mentioned factors have been studied. Besides load capacity, the present paper also includes the exploration of friction, friction coefficient, and position of COP with the effects of altering film ratio. The effects of various parameters on bearings characteristics have been analysed in tabular form and presented graphically. Also, the present work has not been carried out so far by any other researcher with hematite suspension based thin lubrication film under the above circumstances.

Applications of slider bearings: Various slider bearings such as journal bearings, thrust bearings, conical bearings etc. may be used in applications such as construction (expansion supports for bridges), precision tooling (boring and drilling machines, gear cutters, grinders, milling machines), agriculture, automotive, material handling and industrial equipments.

2. BEARING DESIGN, MATHEMATICAL MODEL AND APPROACH

The slider bearing in Figure 1 has a magnetic fluid film of thickness $\hbar$ within pads of length L. The film height $\hbar$ varies from $\hbar_0$ at the outlet to $\hbar_1$ at the inlet. The slider moves with a uniform velocity U_x along x-direction. The lower pad stator of the slider is having a porous matrix of width l and porosity κ backed with a solid barrier.

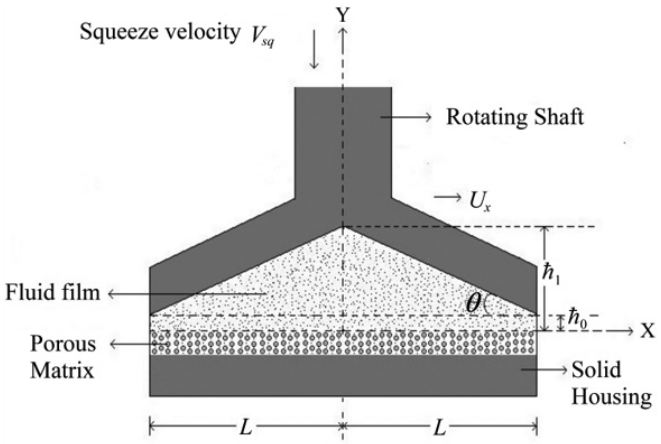

Figure 1. Inclined slider bearing having a porous matrix.

Jenkins model has been employed as a mathematical set of following governing equations and a dynamic Reynolds equation is obtained for inclined slider.

$$\rho\left[\frac{\partial \vec{V}}{\partial t}+(\vec{V}.\nabla)\vec{V}\right] = -\nabla P_r+\mu\nabla^2\vec{V}+\mu_0\left(M.\nabla\right)F+\rho\lambda^2\nabla\times\left(\frac{\tilde{M}}{M}\times M^*\right); \quad (1)$$

$$\nabla.\vec{V}=0; \quad (2)$$

$$\nabla\times F=0,\ F=-\nabla\phi; \quad (3)$$

$$\nabla.\left(F+4\pi M\right)=0; \quad (4)$$

and

$$\beta\frac{D^2\tilde{M}}{Dt^2}=-4\pi p_r\frac{M_s}{\chi_0}\frac{\tilde{M}}{M_s-M}-\frac{2\lambda^2}{M}M^*+F \quad (5)$$

where,

$$M^*=\frac{D\tilde{M}}{Dt}+\frac{1}{2}(\nabla\times\vec{V})\times\tilde{M}. \quad (6)$$

Further, Simpson's one-third rule with a precision of 5 significant digits (rounded to 4 digits) and step size 0.1 is approached to calculate the non-dimensional values for different bearing characteristics.

3. FORMULATION

Employing Ram & Verma[26] on the above governing model, the following resultant equation has been obtained:

$$\frac{\partial^2 V_x}{\partial y^2}=\frac{1}{\mu_v\left(1-\rho\lambda^2\mu_s F/2\mu_v\right)}\frac{\partial}{\partial x}\left(P_r-\frac{\mu_o\mu_s}{2}F^2\right) \quad (7)$$

Now using the boundary slip conditions of Sparrow[28], *et al.* i.e.

$$V_x = U_x \ at \ y = \hbar, \quad V_x = \frac{1}{\tau}\frac{\partial V_x}{\partial y} \quad at \quad y = 0; \tag{8}$$

$\frac{1}{\tau}$ being the slip parameter, the solution of Eqn is obtained as:

$$V_x = \frac{1+\tau y}{1+\tau\hbar}U_x + \frac{\{y(1+\tau\hbar)+\hbar\}(y-\hbar)}{(1+\tau\hbar)2\mu_v\left(1-\rho\lambda^2\mu_s F/2\mu_v\right)}\frac{\partial}{\partial x}\left(P_r - \frac{\mu_o\mu_s}{2}F^2\right) \tag{9}$$

Substitution of V_x in the integral equation for continuity in film region

$$\frac{\partial}{\partial x}\int_0^{\hbar} V_x dy \ + \ V_{y(\hbar)} - V_{y(0)} = 0, \tag{10}$$

yields the following equation

$$\frac{d}{dx}\left[\begin{array}{l}\dfrac{U_x\hbar(2+\tau\hbar)}{2(1+\tau\hbar)} - \\ \dfrac{\hbar^3(4+\tau\hbar)}{12\mu_v(1+\tau\hbar)\left(1-\rho\lambda^2\mu_s F/2\mu_v\right)}\dfrac{d}{dx}\left(P_r - \dfrac{\mu_o\mu_s}{2}F^2\right) \\ + V_{sq}\,x\end{array}\right] = V_{y(0)} \tag{11}$$

considering $V_{y(\hbar)} = V_{sq} = -\frac{dh}{dt}$, the squeeze velocity of the slider in the downward direction.

In the porous matrix, the fluid velocity components due to Ram and Verma[26] are given as

$$v_x = -\frac{\kappa}{\mu_v}\left[\frac{\partial}{\partial x}\left(p_r - \frac{\mu_o\mu_s}{2}F^2\right) + \frac{\rho\lambda^2\mu_s}{2}\frac{\partial}{\partial x}\left(F\frac{\partial V_x}{\partial y}\right)\right], \tag{12}$$

$$v_y = -\frac{\kappa}{\mu_v}\left[\frac{\partial}{\partial y}\left(p_r - \frac{\mu_o\mu_s}{2}F^2\right) - \frac{\rho\lambda^2\mu_s}{2}\frac{\partial}{\partial x}\left(F\frac{\partial V_x}{\partial y}\right)\right], \tag{13}$$

where κ and p_r represents the porosity and the pressure respectively.

The equation of continuity in the porous section yields

$$\frac{\partial^2}{\partial x^2}\left(p_r - \frac{\mu_o\mu_s}{2}F^2\right) + \frac{\partial^2}{\partial y^2}\left(p_r - \frac{\mu_o\mu_s}{2}F^2\right) = 0 \tag{14}$$

and its integration (Morgan-Cameron[29] and Prakash & Vij[30]) athwart the porous region $(-l, \ 0)$ gives

$$\frac{\partial}{\partial y}\left(p_r - \frac{\mu_o\mu_s}{2}F^2\right)_{y=0} = -l\frac{d^2}{dx^2}\left(P_r - \frac{\mu_o\mu_s}{2}F^2\right), \tag{15}$$

Now using Eqn (13), the fluid velocity athwart the porous-film interface is obtained as:

$$V_{y(0)} = v_{y(0)} = -\frac{\kappa}{\mu_v}\left[\begin{array}{l}\left\{\dfrac{\partial}{\partial y}\left(P_r - \dfrac{\mu_o\mu_s}{2}F^2\right)\right\}_{y=0} \\ -\left\{\dfrac{1}{2}\rho\lambda^2\mu_s\dfrac{\partial}{\partial x}\left(F\dfrac{\partial V_x}{\partial y}\right)\right\}_{y=0}\end{array}\right], \tag{16}$$

Using Eqns (9), (15), and (16) in Eqn (11) yields

$$\frac{d}{dx}\left[\left\{\frac{12\kappa l + \dfrac{\hbar^3(4+\tau\hbar) - (3\rho\lambda^2\mu_s\kappa\tau\hbar^2F)/\mu_v}{(1+\tau\hbar)(1-\rho\lambda^2\mu_s F/2\mu_v)}}{}\right\}\frac{d}{dx}\left(P_r - \frac{\mu_o\mu_s}{2}F^2\right)\right] = \left[\frac{6\mu_v U_x\hbar(2+\tau\hbar) - 6U_x\rho\lambda^2\mu_s\kappa\tau F}{1+\tau\hbar} + 12\mu_v V_{sq}x\right], \tag{17}$$

which represents the Reynolds dynamic equation.

Now consider a field applied at an angle θ in the x-direction and vanishing at the inlet &outlet.

$$F_x = F(x)\cos\theta; \ F_y = F(x)\sin\theta, \tag{18}$$

where $\theta = \theta(x, \ y)$ and $F_z = 0$.

F^2 should convince the condition: $F^2(x) = 0$ at $x = 0, \ L$.

So, F^2 can be taken as

$$F^2(x) = K_1 x(L-x), \tag{19}$$

where K_1 is a suitably chosen arbitrary constant. Now Maxwell Equation reduces to

$$\frac{\partial F_y}{\partial x} - \frac{\partial F_x}{\partial y} = 0. \tag{20}$$

Substituting Eqns (18) and (19) into Eqn (20) gives us $\theta(x, \ y)$ and it obeys the following differential equation:

$$\cot\theta\frac{\partial\theta}{\partial x} + \frac{\partial\theta}{\partial y} = -\frac{L-2x}{2(Lx-x^2)}, \tag{21}$$

which yields

$$\cos ec^2\theta = C^2(Lx - x^2) \tag{22}$$

and

$$C(2x-L) = [C^2L^2 - 4\sin(Cy)]^{1/2} \tag{23}$$

remembering that the self-field created due to magnetisation has been ignored.

4. SOLUTION

Introducing the subsequent dimensionless variables:

$$\bar{x} = \frac{x}{L}, \ \bar{\hbar} = \frac{\hbar}{\hbar_0}, \ \bar{P}_r = \frac{P_r\hbar_0^2}{\mu_v U_x L}, \bar{\gamma}^2 = \frac{6\kappa}{\hbar_0^2}, \ \bar{\lambda}^2 = \frac{\rho\lambda^2\mu_s L}{2\mu_v},$$
$$\bar{V}_{sq} = -\frac{2V_{sq}L}{U_x\hbar_0}, \ \bar{\varepsilon} = \frac{\kappa l}{\hbar_0^3}, \ \bar{\mu}_m = \frac{\bar{\mu}_o\mu_s\hbar_0^2 L}{\mu_v U_x}, \ \bar{\tau} = \tau\hbar_0; \tag{24}$$

Equation (17) transforms into

$$\frac{d}{d\bar{x}}\left[\begin{array}{l}\left\{12\bar{\varepsilon} + \dfrac{\bar{\hbar}^3\left(\dfrac{4}{\bar{\tau}} + \bar{\hbar}\right) - \bar{\hbar}^2\bar{\lambda}^2\bar{\gamma}^2\sqrt{\bar{x}(1-\bar{x})}}{\left(\dfrac{1}{\bar{\tau}} + \bar{\hbar}\right)(1-\bar{\lambda}^2\sqrt{\bar{x}(1-\bar{x})})}\right\}\times \\ \dfrac{d}{d\bar{x}}\left(\bar{P}_r - \dfrac{1}{2}\bar{\mu}_m\bar{x}(1-\bar{x})\right)\end{array}\right] = \frac{d}{d\bar{x}}\left[\frac{6\bar{\hbar}\left(\dfrac{2}{\bar{\tau}} + \bar{\hbar}\right) - 2\bar{\lambda}^2\bar{\gamma}^2\sqrt{\bar{x}(1-\bar{x})}}{\left(\dfrac{1}{\bar{\tau}} + \bar{\hbar}\right)} - 6\bar{V}_{sq}\,\bar{x}\right] \tag{25}$$

The Eqn (25) can be written as

$$\frac{d}{d\bar{x}}\left[\bar{A}\frac{d}{d\bar{x}}\left(\bar{P}_r-\frac{1}{2}\bar{\mu}_m\bar{x}(1-\bar{x})\right)\right]=\frac{d\bar{B}}{d\bar{x}} \tag{26}$$

where

$$\bar{A}=12\bar{\varepsilon}+\frac{\bar{\hbar}^3\left(\frac{4}{\bar{\tau}}+\bar{\hbar}\right)-\bar{\hbar}^2\bar{\lambda}^2\bar{\gamma}^2\sqrt{\bar{x}(1-\bar{x})}}{\left(\frac{1}{\bar{\tau}}+\bar{\hbar}\right)(1-\bar{\lambda}^2\sqrt{\bar{x}(1-\bar{x})})} \tag{27}$$

and

$$\bar{B}=\frac{6\bar{\hbar}\left(\frac{2}{\bar{\tau}}+\bar{\hbar}\right)-2\bar{\lambda}^2\bar{\gamma}^2\sqrt{\bar{x}(1-\bar{x})}}{\left(\frac{1}{\bar{\tau}}+\bar{\hbar}\right)}-6\bar{V}_{sq}\,\bar{x} \tag{28}$$

Solving Eqn (26) with boundary conditions,

$$\bar{P}_r(0)=\bar{P}_r(1)=0, \tag{29}$$

the equation for pressure in the film region is acquired as:

$$\bar{P}_r=\frac{1}{2}\bar{\mu}_m\bar{x}(1-\bar{x})+\int_1^x\frac{\bar{B}-\bar{C}}{\bar{A}}d\bar{x} \tag{30}$$

where

$$\bar{C}=\frac{\int_0^1(\bar{B}/\bar{A})d\bar{x}}{\int_0^1(1/\bar{A})d\bar{x}} \tag{31}$$

For an inclined slider bearing

$$\hbar=\hbar_1-(\hbar_1-\hbar_0)x/L\ \Rightarrow\ \bar{\hbar}=r_{i/o}-(r_{i/o}-1)\bar{x} \tag{32}$$

where $r_{i/o}=\hbar_1/\hbar_0$.

The Expressions in dimensionless form for load capacity, friction, coefficient of friction, and position of COP can be obtained as:

$$\bar{W}=\frac{\hbar_0^2W}{\mu_vU_xL^2l}=\frac{\bar{\mu}_m}{12}-\int_0^1\bar{x}\frac{\bar{B}-\bar{C}}{\bar{A}}d\bar{x}, \tag{33}$$

$$\bar{F}_r=\frac{\hbar_0F_r}{\mu_vU_xLl}=\int_0^1\left[\frac{1}{\left(\frac{1}{\bar{\tau}}+\bar{\hbar}\right)}+\frac{\bar{\hbar}\left(\frac{2}{\bar{\tau}}+\bar{\hbar}\right)\bar{B}-\bar{C}}{2\bar{A}\left(\frac{1}{\bar{\tau}}+\bar{\hbar}\right)(1-\bar{\lambda}^2\sqrt{\bar{x}(1-\bar{x})})}\right]d\bar{x}, \tag{34}$$

$$\bar{f}_c=\frac{Lf_c}{\hbar_0}=\frac{\bar{F}_r}{\bar{W}_i}, \tag{35}$$

$$\bar{C}_p=\frac{mean(\bar{x})}{L}=\frac{1}{\bar{W}}\left[\frac{\bar{\mu}_m}{24}-\frac{1}{2}\int_0^1\bar{x}^2\frac{\bar{B}-\bar{C}}{\bar{A}}d\bar{x}\right]. \tag{36}$$

5. RESULTS AND DISCUSSION

Using Simpson's one-third rule, the non-dimensional values for different bearing characteristics resembling load capacity $\bar{W}$, friction $\bar{F}_r$, friction coefficient $\bar{f}_c$ and position of COP $\bar{C}_p$ are computed and displayed in Tables 1-4 and Figs. 2-5.

Table1. Variations in non-dimensional load capacity for various values of material and slip parameters at different values of the squeeze velocity

		$\bar{\lambda}^2\rightarrow$				
	$1/\bar{\tau}\downarrow$	0.02	0.2	0.4	0.8	1.6
$\bar{V}_{sq}=0$	0.02	0.2346	0.2275	0.2195	0.2026	0.1646
	0.03	0.2318	0.2248	0.2169	0.2003	0.1631
	0.04	0.2291	0.2223	0.2145	0.1982	0.1616
$\bar{V}_{sq}=0.2$	0.02	0.2648	0.2564	0.2468	0.2266	0.1810
	0.03	0.2614	0.2531	0.2437	0.2238	0.1792
	0.04	0.2582	0.2500	0.2407	0.2212	0.1774
$\bar{V}_{sq}=0.4$	0.02	0.2951	0.2852	0.2740	0.2505	0.1974
	0.03	0.2911	0.2814	0.2704	0.2473	0.1953
	0.04	0.2874	0.2778	0.2670	0.2443	0.1932

Table 2. Variations in non-dimensional friction for various values of slip and material parameters at different values of the squeeze velocity

		$\bar{\lambda}^2\rightarrow$				
	$1/\bar{\tau}\downarrow$	0.02	0.2	0.4	0.8	1.6
$\bar{V}_{sq}=0$	0.02	0.7599	0.7649	0.7713	0.7874	0.8494
	0.03	0.7536	0.7586	0.7649	0.7806	0.8415
	0.04	0.7476	0.7524	0.7586	0.7740	0.8338
$\bar{V}_{sq}=0.2$	0.02	0.7752	0.7813	0.7890	0.8086	0.8851
	0.03	0.7686	0.7746	0.7822	0.8014	0.8765
	0.04	0.7623	0.7682	0.7756	0.7945	0.8682
$\bar{V}_{sq}=0.4$	0.02	0.7905	0.7976	0.8067	0.8298	0.9208
	0.03	0.7837	0.7907	0.7996	0.8222	0.9115
	0.04	0.7771	0.7839	0.7927	0.8149	0.9025

Table 3. Variations in non-dimensional friction coefficient for various values of slip and material parameters at different values of the squeeze velocity

		$\bar{\lambda}^2\rightarrow$				
	$1/\bar{\tau}\downarrow$	0.02	0.2	0.4	0.8	1.6
$\bar{V}_{sq}=0$	0.02	3.2392	3.3618	3.5142	3.8860	5.1602
	0.03	3.2518	3.3742	3.5262	3.8966	5.1601
	0.04	3.2631	3.3853	3.5370	3.9058	5.1591
$\bar{V}_{sq}=0.2$	0.02	2.9270	3.0472	3.1975	3.5689	4.8895
	0.03	2.9402	3.0603	3.2104	3.5807	4.8919
	0.04	2.9521	3.0722	3.2221	3.5913	4.8934
$\bar{V}_{sq}=0.4$	0.02	2.6789	2.7963	2.9439	3.3123	4.6639
	0.03	2.6921	2.8095	2.9571	3.3248	4.6680
	0.04	2.7042	2.8217	2.9691	3.3361	4.6712

Results given in Tables 1-4 reveals ($\bar{\varepsilon}=0.001$, $\bar{\mu}_m=1.0$, $\bar{\gamma}^2=0.3$, $r_{i/o}=2$) that an enhancement in slip parameter $1/\bar{\tau}$ results a decrease in $\bar{W}$ as well as $\bar{F}_r$ and increase in $\bar{f}_c$ without much affecting $\bar{C}_p$. However, a raise in squeeze velocity $\bar{V}_{sq}$ results an increase in $\bar{W}$ as well as $\bar{F}_r$ and decrease in $\bar{f}_c$ shifting $\bar{C}_p$ slightly towards the outlet. Therefore, the effects of $1/\bar{\tau}$ are exactly opposite to that of the $\bar{V}_{sq}$.

Table 4. Variations in non-dimensional position of COP for various values of slip and material parameters at different values of the squeeze velocity

		$\bar{\lambda}^2 \rightarrow$				
	$1/\bar{\tau} \downarrow$	0.02	0.2	0.4	0.8	1.6
$\bar{V}_{sq} = 0$	0.02	0.5437	0.5426	0.5412	0.5378	0.5254
	0.03	0.5432	0.5421	0.5407	0.5373	0.5250
	0.04	0.5427	0.5416	0.5402	0.5368	0.5247
$\bar{V}_{sq} = 0.2$	0.02	0.5465	0.5455	0.5442	0.5410	0.5285
	0.03	0.5459	0.5449	0.5437	0.5405	0.5281
	0.04	0.5454	0.5444	0.543`	0.5400	0.5277
$\bar{V}_{sq} = 0.4$	0.02	0.5487	0.5478	0.5466	0.5436	0.5311
	0.03	0.5481	0.5472	0.5461	0.5430	0.5306
	0.04	0.5476	0.5467	0.5455	0.5425	0.5302

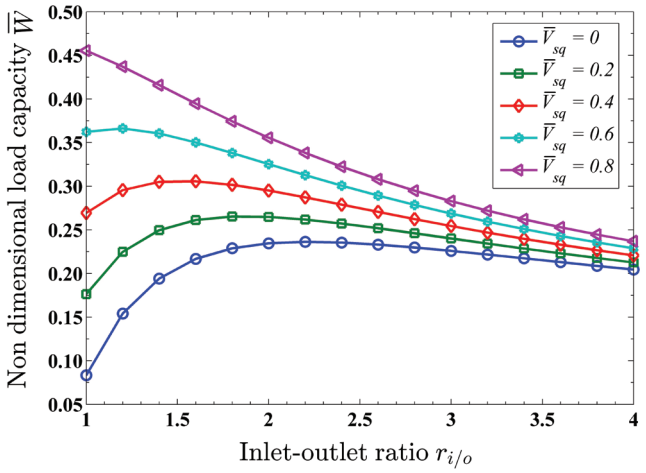

Figure 2. Inlet-outlet ratio vs. Load capacity for different values of squeeze velocity.

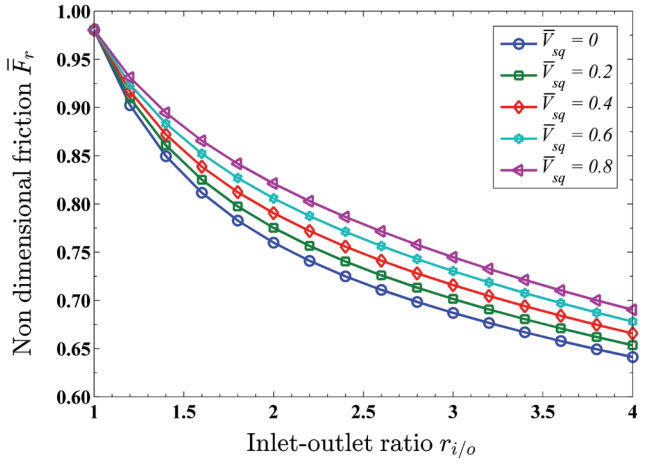

Figure 3. Inlet-outlet ratio vs. Friction for different values of squeeze velocity.

Further, it is also noted that an increase in the material parameter $\bar{\lambda}^2$ causes a decrease in $\bar{W}$ and increase in $\bar{F}_r$ as well as $\bar{f}_c$ shifting $\bar{C}_p$ slightly towards the inlet.

The variations in $\bar{W}$, $\bar{F}_r$, $\bar{f}_c$ and $\bar{C}_p$ w.r.t. the inlet-outlet ratio $r_{i/o}$ of the lubricant film between the lower and upper pad of the slider are plotted in Figures 2-5 at $\bar{\varepsilon} = 0.001$, $\bar{\mu}_m = 1.0$, $\bar{\gamma}^2 = 0.3$, $\bar{\lambda}^2 = 0.02$, $1/\bar{\tau} = 0.02$.

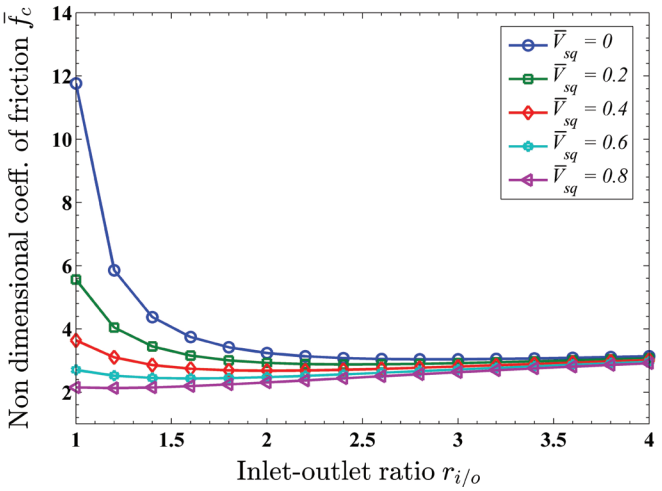

Figure 4. Inlet-outlet ratio vs. Friction coefficient for different values of squeeze velocity.

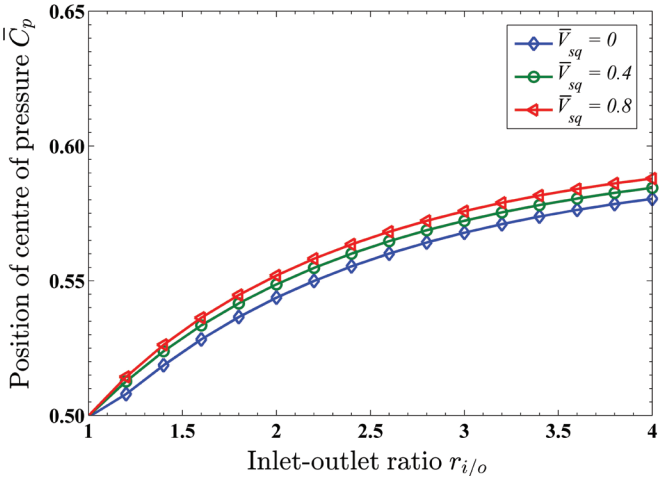

Figure 5. Inlet-outlet ratio vs. Position of COP for different values of squeeze velocity.

It is seen from Figs. 2-5, that there is an appreciation in $\bar{W}$ with an increase in the squeeze velocity. Also, there is an optimum value of $r_{i/o}$ after that $\bar{W}$ starts diminishing means at this optimum value, there is a reversal in trends. The optimum values of $r_{i/o}$ for which $\bar{W}$ is maximum, are different at different values of $\bar{V}_{sq}$. For the squeeze velocity, $\bar{V}_{sq} = 0,\ 0.2,\ 0.4,\ 0.6$ *and* 0.8, these optimum values of $r_{i/o}$ are 2.2, 1.8, 1.6, 1.2 and 1 respectively.

Further, $\bar{F}_r$ decreases due to increase in $r_{i/o}$ while it increases due to increase in $\bar{V}_{sq}$. The effect of squeeze velocity $\bar{V}_{sq}$ on friction is negligible for lower values of the inlet-outlet ratio. It is also noted that $\bar{f}_c$ reduces due to increase in $\bar{V}_{sq}$ and $r_{i/o}$. The squeeze effects are significant for smaller values of $r_{i/o}$ and a drastic fall in $\bar{f}_c$ can be observed, if the squeeze velocity is introduced. The position of $\bar{C}_p$ is shifted away from the inlet if we increase $r_{i/o}$ as well as $\bar{V}_{sq}$.

Validation with existing results: In Tables 1-4, the obtained results for $\bar{V}_{sq} = 0$ are in a complete consonance to Shah & Bhatt[24]. Also, the trends in Fig. 2 for optimum value of the inlet-outlet ratio are similar to Ram[27], *et al.*.

6. CONCLUSIONS

As the squeeze velocity has increased, the load capacity has enhanced and the friction coefficient has reduced significantly. However, reversal trends have been observed for slip and material parameters. Therefore, tuning can be made between the squeeze velocity vs. the slip velocity and material parameter to reduce the friction coefficient and hence to improve the load capacity.

The optimum value of the film ratio is 2.2 for zero squeeze velocity and is 1 for the higher value of squeeze velocity ≥ 0.8 . Therefore, it is recommended that the inlet-outlet ratio of the slider should be set up in accordance with the magnitude of the squeeze velocity to attain the maximum load capacity.

It has been noted that an increase in the material parameter shifts the position of COP slightly towards the inlet whereas an increase in squeeze velocity and inlet-outlet ratio, shifts the same slightly towards the outlet. So, the position of COP can be balanced by choosing the inlet-outlet ratio and the squeeze velocity according to the material properties of the slider.

REFERENCES

1. Ram, P. & Kumar, A. Analysis of heat transfer and lifting force in a ferro-nanofluid based porous inclined slider bearing with slip conditions.*Nonlinear Eng.,* 2018, **8**(1), 206–15. doi: 10.1515/nleng-2018-0014
2. Ram, P. & Kumar, A. Investigation of thermal effects in a ferrofluid-based porous inclined slider bearing with slip conditions. *In* Numerical Heat Transfer and Fluid Flow2019: Lect. Notes Mech. Eng., Springer, Singapore, 2019. doi: 10.1007/978-981-13-1903-7_6
3. Li, X.; Shinshi, T.; Hijikata, W. & Morimoto, Y. Development of a suspension type sliding planar motion table using magnetic fluid lubrication. *Rev. Sci. Instrum.,* 2016, **87**(6), 065003. doi: 10.1063/1.4953653
4. Ram, P. & Kumar, V. Ferrofluid flow with magnetic field-dependent viscosity due to rotating disk in porous medium. *Int. J. Appl. Mech.,* 2012, **4**(4), 1250041. doi: 10.1142/S175882511250041X
5. Ram. P.; Joshi, V.K.; Makinde, O.D. & Kumar A. Convective boundary layer flow of magnetic nanofluids under the influence of geothermal viscosity. *Defect Diffus. Forum.,* 2018, **387**, 296–307. doi: 10.4028/www.scientific.net/DDF.387.296
6. Ellahi, R.; Tariq, M.H. & Hassan, M. On boundary layer nano-ferro liquid flow under the influence of low oscillating stretchable rotating disk. *J. Mol.Liq.,* 2017, **229**, 339–45. doi: 10.1016/j.molliq.2016.12.073
7. Lin, J.R. Derivation of ferrofluid lubrication equation of cylindrical squeeze films with convective fluid inertia forces and application to circular disks. *Tribol. Int.,* 2012, **49**, 110–5. doi: 10.1016/j.triboint.2011.11.006
8. Lin, J.R.; Lu, R.F.; Lin, M.C. & Wang, P.Y. Squeeze film characteristics of parallel circular disks lubricated by ferrofluids with non-Newtonian couple stresses. *Tribol. Int.,* 2013, **61**, 56–61. doi: 10.1016/j.triboint.2012.12.001
9. Verma, P.D.S. &Ram, P. On the low-Reynolds number magnetic fluid flow in a helical pipe. *Int. J. Eng. Sci.,* 1993, **31**(2), 229–39. doi:10.1016/0020-7225(93)90036-T
10. Huang, W. & Wang, X. Ferrofluids lubrication: a status report. *Lubr. Sci.,* 2016, **28**(1), 3–26. doi: 10.1002/ls.1291
11. Kumar, V. & Sharma, S.C. Magneto-hydrostatic lubrication of thrust bearings considering different configurations of recess. *Ind. Lubr. Tribol.,* 2019, **71**(7), 915–23. doi: 10.1108/ILT-10-2018-0370
12. Zoupas, L.; Wodtke, M.; Papadopoulos, C.I. & Wasilczuk, M. Effect of manufacturing errors of the pad sliding surface on the performance of the hydrodynamic thrust bearing. *Tribol. Int.,* 2019, **134**, 211–20. doi: 10.1016/j.triboint.2019.01.046
13. Amalraj, I.J.; Narasimman, S. & Kandasamy, A. Inertia effects in rheodynamic lubrication of an externally pressurized thrust bearing using bingham lubricant with sinusoidal injection. *J. Appl. Fluid Mech.,* 2013, **6**(4), 609–16 doi: 10.36884/jafm.6.04.19554
14. Laghrabli, S.; Khlifi, M.E.; Nabhani, M. & Bou-Saïd, B. Ferrofluid lubrication of finite journal bearings using Jenkins model. *Lubr. Sci.,* 2017, **29**(7), 441–54. doi: 10.1002/ls.1379
15. Laghrabli, S.; Khlifi, M.E.; Nabhani, M. & Bou-Saïd, B. Static characteristics of ferrofluid finite journal bearing considering rotational viscosity effect. *Lubr. Sci.,* 2017, **29**(4), 203–26. doi: 10.1002/ls.1364
16. Lin, Q.; Bao, Q.; Li, K.; Khonsari M.M. & Zhao, H. An investigation into the transient behavior of journal bearing with surface texture based on fluid-structure interaction approach. *Tribol. Int.,* 2018, **118**, 246–55. doi: 10.1016/j.triboint.2017.09.026
17. Lin, Q.; Wei, Z.; Zhang, Y. &Wang, N. Effects of the slip surface on the tribological performances of high-speed hybrid journal bearings. *Proc. Inst. Mech. Eng. Part J J. Eng. Tribol.,* 2016, **230**(9), 1149–56. doi: 10.1177/1350650116630202
18. Sinha, P.; Chandra, P. &Bhartiya, S. Analysis of a non-constant gap externally pressurized conical bearing with temperature and pressure dependent viscosity. *Proc. Inst. Mech. Eng. Part C: J. Mech. Eng.,* 2000, **214**(5), 699–710. doi: 10.1243/0954406001523704
19. Mouda, M.; Nabhani, M. & El-Khlifi, M. Effect of non-Newtonian magneto-elastohydrodynamic on performance characteristics of slider-bearings. *Ind. Lubr. Tribol.,* 2019, **71**(10), 1158–65. doi: 10.1108/ILT-11-2018-0416.
20. Patel, K.C. & Gupta, J.L. Hydrodynamic lubrication of a porous slider bearing with slip velocity. *Wear,* 1983, **85**(3), 309–17.

doi: 10.1016/0043-1648(83)90225-9
21. Lin, J.R. & Chu, L.M. Dynamic characteristics of exponential slider bearings lubricated with a ferrofluid – Shliomis model. *Ind. Lubr. Tribol.,* 2018, **70**(4), 673–9. doi: 10.1108/ILT-03-2016-0063
22. Wu, J.; Wang, L.; He, T.; Gu, L.; Zhang, C. & Lu, Y. Investigation on the angular contact ball bearings under low speed and heavy load with coupled mixed lubrication and quasi-dynamic analysis. *Lubr. Sci.,* 2020, **32**(3), 108–20. doi: 10.1002/ls.1490
23. Han, K.; Li, J.; Wang, Q.; Chen, W. & Xue, J. Study on oil film pressure distribution and load capacity of textured rolling bearings. *Ind. Lubr. Tribol.,* 2020, **72**(7), 961–7. doi: 10.1108/ILT-02-2020-0055
24. Shah, R.C.& Bhat, M.V. Ferrofluid lubrication in porous inclined slider bearing with velocity slip. *Int. J. Mech. Sci.,* 2002, **44**(12), 2495–502. doi: 10.1016/S0020-7403(02)00187-X
25. Agrawal, V.K. Magnetic-fluid-based porous inclined slider bearing. *Wear,* 1986, **107**(2), 133–9. doi: 10.1016/0043-1648(86)90023-2
26. Ram, P. & Verma, P.D.S. Ferrofluid lubrication in porous inclined slider bearing. *Indian J. Pure Appl. Math.,* 1999, **30**(12), 1273–82.
27. Ram, P.; Kumar, A.; Makinde, O.D.; Kumar, P. & Joshi, V.K. Performance Analysis of magnetite nano-suspension based porous slider bearing with varying inclination and slip parameter. *Diffus. Found.,* 2017, **11**, 11–21. doi: 10.4028/www.scientific.net/df.11.11
28. Sparrow, E.M.; Beavers, G.S. & Hwang, I.T. Effect of velocity slip on porous-walled squeeze films. *J. Lubr. Technol.,* 1972, **94**(3), 260–4. doi: 10.1115/1.3451704
29. Morgan, V.T. & Cameron, A. Mechanism of lubrication in porous metal bearings. *In* Proceedings of the Conference on Lubrication and Wear 1957: Inst. Mech. Eng. London 1957, **89**, 151-7.
30. Prakash, J. & Vij, S.K. Hydrodynamic lubrication of a porous slider. *J. Mech. Eng. Sci.,* 1973, **15**(3), 232–4. doi: 10.1243/JMES_JOUR_1973_015_039_02

CONTRIBUTORS

Dr Paras Ram did his post-graduation from Department of Mathematics, Kurukshetra University Kurukshetra and PhD from Regional Engineering College (REC) Kurukshetra (Now NIT Kurukshetra). At present, he has been working as a Sr. Professor in the Department of Mathematics, NIT-Kurukshetra. His research interests primarily include Fluid Dynamics: MHD, FHD and Lubrication theory. He has published more than 75 research articles in esteemed journals & conferences.
In the current study, he has worked as a mentor. He has reviewed and validated the results and given valuable suggestions to improve the quality of work.

Mr Anil Kumar did his post-graduation from Department of Mathematics, Kurukshetra University Kurukshetra. He is currently pursuing his PhD from the Department of Mathematics, NIT-Kurukshetra. He has published 4 research papers in esteemed journals & conferences.
In the current study, he is actively involved in providing technical and scientific inputs for computational analysis of data and contributed to writing and editing the paper.